ISSN 1560-3547, Regular and Chaotic Dynamics, 2010, Vol. 15, Nos. 2–3, pp. 107–126. © Pleiades Publishing, Ltd., 2010.

L.P. SHILNIKOV–75
Special Issue

Rigorous and Accurate Enclosure of Invariant Manifolds on Surfaces

A. Wittig[1*], M. Berz[1], J. Grote[1***], K. Makino[1****], and S. Newhouse[2*****]**

[1] *Department of Physics and Astronomy*
Michigan State University, East Lansing, MI 48824, USA

[2] *Department of Mathematics*
Michigan State University, East Lansing, MI 48824, USA

Received December 20, 2009; accepted January 14, 2010

Abstract—Knowledge about stable and unstable manifolds of hyperbolic fixed points of certain maps is desirable in many fields of research, both in pure mathematics as well as in applications, ranging from forced oscillations to celestial mechanics and space mission design. We present a technique to find highly accurate polynomial approximations of local invariant manifolds for sufficiently smooth planar maps and rigorously enclose them with sharp interval remainder bounds using Taylor model techniques. Iteratively, significant portions of the global manifold tangle can be enclosed with high accuracy. Numerical examples are provided.

MSC2000 numbers: 37C05

DOI: 10.1134/S1560354710020024

Key words: Taylor model, invariant manifold, hyperbolicity, homoclinic point

To Leonid Pavlovich Shilnikov
on the occasion of his seventy-fifth birthday

1. INTRODUCTION

One of the richest questions that can be asked about an arbitrary given dynamical system (for brevity, we will only consider maps from now on) concerns the existence of hyperbolic fixed and periodic points and the structure of their respective stable and unstable manifolds. Knowledge about if and how these manifolds intersect yields insight into many telling characteristics of the system, such as homo- and heteroclinic phenomena, topological entropy and horseshoe dynamics. The manifold structure can be arguably complicated and it has long been a challenge to develop quality numerical tools to investigate it.

By their very nature, these invariant manifolds are transports under the map (or its respective inverse) of local invariant manifolds which can be shown to exist near a fixed point by virtue of the Invariant Manifold Theorem (Hadamard–Perron Theorem). We present a technique based on Taylor model arithmetic which allows, under quite general assumptions, to compute very accurate high-order polynomial approximations of the local manifolds using nonlinear normal form transformations, and to outfit these polynomials in a subsequent step with interval remainder bounds which rigorously enclose the local manifolds.

*E-mail: wittigal@msu.edu
**E-mail: berz@msu.edu
***E-mail: grotejoh@msu.edu
****E-mail: makino@msu.edu
*****E-mail: newhouse@math.msu.edu

1.1. Invariant Manifolds

Let $f : \mathbb{R}^\nu \longrightarrow \mathbb{R}^\nu$ be a $\mathcal{C}^r$-diffeomorphism and let p_0 be a periodic point of f. We may assume that p_0 is actually a fixed point of f by taking an appropriate power of the map. Further assume that p_0 is hyperbolic, i.e. that the $Df(p_0)$ does not have any eigenvalues of norm 1. More specifically, let $\lambda_1^u, \ldots, \lambda_k^u$ be the k unstable eigenvalues ($|\lambda_i^u| > 1$ for $1 \leqslant i \leqslant k$) and $\lambda_1^s, \ldots, \lambda_l^s$ be the l stable eigenvalues ($|\lambda_i^s| < 1$ for $1 \leqslant i \leqslant l$). There exists a direct sum decomposition $\mathbb{R}^\nu = E_{p_0}^u \oplus E_{p_0}^s$ of unstable and stable subspaces at p_0 such that $Df|_{E_{p_0}^{u,s}}$ has eigenvalues $\lambda_j^{u,s}$.

Consider the stable and unstable sets

$$\mathcal{W}^s(p_0) = \{x \in \mathbb{R}^\nu : f^k(x) \longrightarrow p_0 \text{ as } k \to \infty\},$$
$$\mathcal{W}^u(p_0) = \{x \in \mathbb{R}^\nu : f^{-k}(x) \longrightarrow p_0 \text{ as } k \to \infty\}.$$

The following theorem states that $\mathcal{W}^s(p_0)$ and $\mathcal{W}^u(p_0)$ are actually manifolds with inherited smoothness from f.

Theorem 1 (Invariant manifold theorem). *Under the above assumptions, $\mathcal{W}^s(p_0)$ and $\mathcal{W}^u(p_0)$ are $\mathcal{C}^r$-injectively immersed copies of $E_{p_0}^s$ and $E_{p_0}^u$ respectively. Furthermore, $\mathcal{W}^s(p_0)$ ($\mathcal{W}^u(p_0)$) is tangent to $E_{p_0}^s$ ($E_{p_0}^u$) at p_0.*

1.2. Taylor Models

We begin with a brief review of some elements of Taylor model methods that are needed in the ensuing discussion, and we restrict ourselves to the plane. More details about the underlying methods can be found in [9, 11] and references therein.

Definition 1 (Taylor Model). *Let $D \subset \mathbb{R}^2$ be an interval box, let $P : \mathbb{R}^2 \to \mathbb{R}$ be a polynomial of order n in two variables, and let $I \subset \mathbb{R}$ be an interval. We call the pair (P, I) a Taylor Model of order n. Let $f : D \to \mathbb{R}$ be a function. We say the Taylor Model (P, I) is a Taylor Model representation of f on D if*

$$f(x) \in P(x) + I \ \forall\, x \in D.$$

We then say that (P, I) encloses f over D, or that (P, I) is a Taylor Model enclosure of f, or that f is contained in (P, I). The interval I is often referred to as the remainder interval of (P, I).

We also use the intuitive notational convention $P + I$ for (P, I).

Thus the polynomial P is used to "model" the behavior of the function f over the domain D. Furthermore, and importantly for our further arguments, the range of f over D is enclosed in the set theoretical sum of the set describing the range of P over D and the set I. The elementary theory of Taylor's formula with remainder entails that such approximations can be quite accurate in practice. Indeed, letting $|A| = \sup\limits_{x,y \in A} (|x - y|)$ denote the diameter of the compact set A, we have the following

Remark 1. If f is at least $(n + 1)$ times continuously differentiable, $z \in D$, and P is the $n-$th order Taylor polynomial of f centered at z, then one can choose an interval I_D such that (P, I_D) is a Taylor Model enclosure of f on D and

$$|I| = O(|D|^{n+1}) \text{ as } |D| \to 0.$$

For practical calculations, the question now is how do we arrive at a suitable P for a given f of interest. If f is given by elementary arithmetic operations, as is the case with the Hénon map which we introduce as an example later, it is possible to build up Taylor models for more complicated objects from those of simpler ingredients by use of purely arithmetic operations. To this end we introduce various definitions. First, for real intervals I_1 and I_2 and the real number c, we define "interval arithmetic" $I_1 + I_2$ and $I_1 \cdot I_2$ as well as $c \cdot I_1$ in the conventional set theoretical sense (see e.g. [14]). We are then ready for the following

Definition 2 (Elementary Taylor Model Arithmetic). *Let (P_1, I_1) and (P_2, I_2) be Taylor models of order $n \in \mathbb{N}$ over the domain D. We define addition, scalar multiplication, and multiplication of Taylor models as follows:*

$$(P_1, I_1) + (P_2, I_2) = (P_1 + P_2, I_1 + I_2)$$
$$c \cdot (P, I) = (c \cdot P, c \cdot I) \text{ for any } c \in \mathbb{R}, \text{ and}$$
$$(P_1, I_1) \cdot (P_2, I_2) = (P_{1\cdot 2}, I_{1\cdot 2})$$

where $P_{1\cdot 2}$ is the part of the polynomial $P_1 \cdot P_2$ up to order n, P_e is the part of the polynomial $P_1 \cdot P_2$ of order $(n+1)$ to $2n$, and

$$I_{1\cdot 2} = I_1 \cdot I_2 + B(P_e) + B(P_1) \cdot I_2 + B(P_2) \cdot I_1.$$

$B(P)$ denotes an interval range bound for the polynomial P, i.e.

$$P(x) \in B(P) \, \forall \, x \in D.$$

Several remarks are in order. First, we note that while there may be many choices for obtaining a "bound" B of a given polynomial P, for our purposes we merely require that the bound is at least as sharp as what is obtained by evaluating P in interval arithmetic over the domain interval D. Furthermore, we extend the definitions to vector-valued functions in a similar way, where the corresponding Taylor model arithmetic operations happen componentwise. Finally, the question arises what these definitions on Taylor models have to do with the functions they describe. This is addressed by the following

Proposition 1. *Let $f_1, f_2 : D \subset \mathbb{R}^2 \to \mathbb{R}$ be functions. If (P_1, I_1) and (P_2, I_2) are Taylor Model representations of f_1 and f_2 over the domain D, respectively. then $(P_1, I_1) + (P_2, I_2)$ is a Taylor model representation of $f_1 + f_2$, over D, $(P_1, I_1) \cdot (P_2, I_2)$ is a Taylor model representation of $f_1 \cdot f_2$, over D, and for any scalar c, $c \cdot (P_1, I_1)$ is a Taylor model representation of $c \cdot f_1$ over D.*

The details of the proofs rest on elementary set theoretical operations; they can be found for example in [9–11]. These references also contain information on more advanced operations, including common intrinsic functions and implicit functions. It is also possible to obtain rigorous enclosures of flows of ODEs [2, 3, 12, 13].

Thus, the proposition provides a simple mechanism to determine Taylor models for complicated functions from those comprising parts of these functions. Furthermore, the operations are particularly suitable for automated execution on a computer, since they involve only finitely many steps of elementary operations of coefficients. Based on this operation, we use the following notation:

Definition 3. *Let F be a function comprised of finitely many operations supported in Taylor model arithmetic. Let (P, I) be a Taylor model. Then we define*

$$F\left((P, I)\right)$$

to be the Taylor model obtained by executing the individual arithmetic steps of F in Taylor model arithmetic.

Apparently, if (P, I) is a Taylor model of a function f, then the Taylor model $F\left((P, I)\right)$ so obtained is a Taylor model for the function composition $F \circ f$.

To conclude, we note that since computers are not able to represent real numbers accurately because of finite significant (mantissa) length, in order to maintain mathematical rigor, it is important to account for round-off errors:

Remark 2 (Rigorous Computer Arithmetic). By careful consideration of the mathematical requirements of rounding properties of floating point computer arithmetic, it is possible to obtain rigorous Taylor model enclosures for sums, products and scalar products of functions by accounting for all round-off errors in the remainder intervals of the Taylor models.

Complete details on this topic can be found in [11, 15].

To conclude our introductory description of Taylor models, we remark that for a complicated function or a large domain D, one single Taylor model will not be able to describe its behavior with sufficient accuracy because of inefficient convergence properties of the Taylor expansion. So for this purpose it is important to split the actual domain D into a suitable finite collection of subdomains D_i such that D lies in the union of these D_i, and apply the methods on these subdomains.

2. HIGH-ORDER APPROXIMATION OF THE LOCAL MANIFOLD

A technique for the explicit construction of polynomial approximations of invariant manifolds can be obtained from the fact that the manifold parametrizations can be chosen in such a way that they obey an eigenvalue scaling law, described below in (2.2). In the planar case, one can relatively simply derive the coefficients of the polynomial expansions of the manifolds. These techniques are standard and are covered in great detail in [4–8].

For ease of notation, let f_n denote the Taylor expansion of a sufficiently differentiable function f around $(0,0)$ to order n, and let $f =_n g$ for two sufficiently differentiable functions f and g denote agreement of their Taylor expansions around $(0,0)$ up to order n. Note that $=_n$ is an equivalence relation.

In the following, let $g : \mathbb{R}^2 \supseteq D \longrightarrow \mathbb{R}^2$ denote a planar C^{r+1} diffeomorphism for some $r > 1$ with a hyperbolic fixed point $p \in D$, here assumed to be at the origin. We further assume that the map g has a diagonal linear part, the eigenvector corresponding to the unstable eigenvalue λ_u, satisfying $|\lambda_u| > 1$ coincides with the x_1-axis, and the eigenvector corresponding to the stable eigenvalue λ_s, satisfying $|\lambda_s| < 1$ coincides with the x_2-axis.

We define the diffeomorphism f to be a polynomial approximation of g to order r, satisfying $f =_r g$. Thus, f can be written as

$$f_1(x_1, x_2) = \lambda_u x_1 + \tilde{f}_1(x_1, x_2),$$
$$f_2(x_1, x_2) = \lambda_s x_2 + \tilde{f}_2(x_1, x_2),$$

where $\tilde{f} = \left(\tilde{f}_1, \tilde{f}_2\right)$ is a polynomial containing only terms of order 2 or higher.

It is well known that the unstable manifold of f can be parameterized by a curve $\gamma^u : \mathbb{R} \longrightarrow \mathbb{R}^2$ satisfying

$$f(\gamma^u(t)) = \gamma^u(\lambda_u t). \tag{2.1}$$

The following induction provides a constructive algorithm to generate an nth order polynomial curve satisfying (2.1) up to some order $n \leqslant r$, thus approximating γ^u. An analogous algorithm can be performed for the stable manifold.

Denote by

$$\gamma_1^{u,n}(t) = \sum_{i=1}^{n} \alpha_i t^i = \gamma_1^{u,n-1}(t) + \alpha_n t^n,$$
$$\gamma_2^{u,n}(t) = \sum_{i=1}^{n} \beta_i t^i = \gamma_2^{u,n-1}(t) + \beta_n t^n,$$

the components of the nth order polynomial approximation of γ^u. We claim that for $n \geqslant 1$ the α_n, β_n can be chosen so that

$$f(\gamma^{u,n}(t)) =_n \gamma^{u,n}(\lambda_u t). \tag{2.2}$$

For $n = 1$, let $\alpha_1 = 1$ and $\beta_1 = 0$. Thus, $\gamma_1^{u,1}(t) = t$, and $\gamma_2^{u,1}(t) = 0$. We see that in fact $\dot{\gamma}^{u,n}(0) = (1,0)^T$ is tangent to the x_1-axis at the origin for every $n \in \mathbb{N}$. Furthermore, we have that

$$f_1(\gamma^{u,1}(t)) = f_1(t,0) = \lambda_u t + \tilde{f}_1(\gamma^{u,1}(t)) =_1 \lambda_u t,$$
$$f_2(\gamma^{u,1}(t)) = f_2(t,0) = \tilde{f}_2(\gamma^{u,1}(t)) =_1 0,$$

since $\tilde{f}$ has no linear part, and thus $f(\gamma^{u,1}(t)) =_1 \gamma^{u,1}(\lambda_u t)$.

For the induction step, assume α_j, β_j, $1 \leqslant j \leqslant n-1$ have been chosen so that

$$f(\gamma^{u,n-1}(t)) =_{n-1} \gamma^{u,n-1}(\lambda_u t). \tag{2.3}$$

Observe that

$$\tilde{f}\left(\gamma_1^{u,n}(t), \gamma_2^{u,n}(t)\right) =_n \tilde{f}\left(\gamma_1^{u,n-1}(t), \gamma_2^{u,n-1}(t)\right). \tag{2.4}$$

Indeed this is the case since $\tilde{f}$ is a polynomial with terms of order 2 and higher, so the nth order terms of $\gamma^{u,n}$ do not contribute to the terms of $\tilde{f}\left(\gamma_1^{u,n}(t), \gamma_2^{u,n}(t)\right)$ of order n or lower, since $\gamma^{u,n}$ has no constant part.

By inserting $\gamma^{u,n}$ into condition (2.2), and using (2.4) we thus find

$$\lambda_u \gamma_1^{u,n-1}(t) + \lambda_u \alpha_n t^n + \tilde{f}_1\left(\gamma_1^{u,n-1}(t), \gamma_2^{u,n-1}(t)\right) =_n \gamma_1^{u,n-1}(\lambda_u t) + \lambda_u^n \alpha_n t^n$$
$$\lambda_s \gamma_2^{u,n-1}(t) + \lambda_s \beta_n t^n + \tilde{f}_2\left(\gamma_1^{u,n-1}(t), \gamma_2^{u,n-1}(t)\right) =_n \gamma_2^{u,n-1}(\lambda_u t) + \lambda_u^n \beta_n t^n.$$

By the induction assumption (2.3), all terms of order up to $n-1$ in the left and right expressions are equal, so we may cancel them. Rearranging the remaining terms of exact order n, and denoting by $S_1^{(n)}$ and $S_2^{(n)}$ the sum of the coefficients of terms of exact order n in $\tilde{f}_1\left(\gamma_1^{u,n-1}(t), \gamma_2^{u,n-1}(t)\right)$ and $\tilde{f}_2\left(\gamma_1^{u,n-1}(t), \gamma_2^{u,n-1}(t)\right)$, we obtain

$$(\lambda_u - \lambda_u^n) \cdot \alpha_n t^n = -S_1^{(n)} t^n,$$
$$(\lambda_s - \lambda_u^n) \cdot \beta_n t^n = -S_2^{(n)} t^n,$$

and hence, because $(\lambda_\sigma - \lambda_u^n) \neq 0 \ \forall n = 2, 3, 4 \ldots, \ \sigma = u, s$ due to hyperbolicity, we can set

$$\alpha_n = -\tfrac{S_1^{(n)}}{(\lambda_u - \lambda_u^n)}, \ \beta_n = -\tfrac{S_2^{(n)}}{(\lambda_s - \lambda_u^n)}. \tag{2.5}$$

With those coefficients, $\gamma^{u,n}$ also satisfies condition (2.2), and the induction is complete.

The construction (2.5) is fully explicit and inductive, since computation of α_n and β_n only requires knowledge of the α_i, β_i for $1 \leqslant i \leqslant n-1$. The method is furthermore particularly easy to carry out on a computer in that it only requires the availability of polynomial arithmetic.
Also note that for eigenvalues sufficiently different from unity the construction is also numerically stable, since then $\lambda_u - \lambda_u^n$ and $\lambda_s - \lambda_u^n$ are never close to zero.

3. VERIFIED ENCLOSURE OF THE LOCAL MANIFOLD

3.1. Construction of Verified Local Invariant Curve Enclosures

In the previous section a technique to find a polynomial approximation for a local part of the unstable curve near a hyperbolic fixed point was introduced.

In the following we describe how such a polynomial approximation can be extended to a two-dimensional Taylor Model "tube" that rigorously encloses the true invariant manifold.

Throughout this section let $\mathbb{R}^2$ denote the Euclidean plane with coordinates (x_1, x_2) and let $f : \mathbb{R}^2 \supset D \longrightarrow \mathbb{R}^2$ be a C^1 diffeomorphism with a hyperbolic fixed point at the origin $(0,0)$. We assume that the dominating eigenvector with eigenvalue λ_u with $|\lambda_u| > 1$ lies in the direction of the positive x_1-axis, and the minor one with eigenvalue λ_s ($|\lambda_s| < 1$) lies in the direction of the positive x_2-axis. Replacing f by f^2 if necessary, we may assume that λ_u and λ_s is positive.

Given a neighborhood V of the origin $(0,0)$, we let W_V^u denote the connected component (i.e., largest connected subset) of $W^u((0,0)) \bigcap V$ which contains $(0,0)$.

It will be convenient to consider the notion of slopes:

Definition 4. *A differentiable curve $\gamma \subset \mathbb{R}^2$ parametrized as $\gamma(t) = (\gamma_1(t), \gamma_2(t))$, with t in some closed interval $I \subset \mathbb{R}$, such that $\dot{\gamma}_1(t) \neq 0 \ \forall t \in I$ is called regular. For regular curves, we define the slope s_γ as*

$$s_\gamma(t) = \frac{\dot{\gamma}_2(t)}{\dot{\gamma}_1(t)}.$$

There is a simple transformation law describing how the derivatives and the slope of a regular curve change under iteration by a C^1 diffeomorphism $f : \mathbb{R}^2 \to \mathbb{R}^2$. For an initial curve $\gamma = (\gamma_1, \gamma_2)$, we denote the transformed curve $\eta := f(\gamma) = (\eta_1, \eta_2)$ and observe that

$$\dot{\eta}(t) = Df(\gamma(t)) \cdot \dot{\gamma}(t)$$

or componentwise

$$\begin{aligned} \dot{\eta}_k(t) &= \partial_1 f_k(\gamma(t)) \cdot \dot{\gamma}_1(t) + \partial_2 f_k(\gamma(t)) \cdot \dot{\gamma}_2(t) \\ &= (\partial_1 f_k(\gamma(t)) + \partial_2 f_k(\gamma(t)) \cdot s_\gamma(t)) \cdot \dot{\gamma}_1(t) \quad \text{for } k = 1, 2 \end{aligned} \tag{3.1}$$

We thus obtain the new slope

$$\begin{aligned} s_\eta(t) &= \frac{\partial_1 f_2(\gamma(t)) \cdot \dot{\gamma}_1(t) + \partial_2 f_2(\gamma(t)) \cdot \dot{\gamma}_2(t)}{\partial_1 f_1(\gamma(t)) \cdot \dot{\gamma}_1(t) + \partial_2 f_1(\gamma(t)) \cdot \dot{\gamma}_2(t)} \\ &= \frac{\partial_1 f_2(\gamma(t)) + \partial_2 f_2(\gamma(t)) \cdot s_\gamma(t)}{\partial_1 f_1(\gamma(t)) + \partial_2 f_1(\gamma(t)) \cdot s_\gamma(t)}. \end{aligned} \tag{3.2}$$

Let E be a parameterized curvilinear rectangle, i.e. the image of the unit square under a polynomial embedding $P : [-1, 1]^2 \longrightarrow \mathbb{R}^2$. Sometimes we abuse the language, and simply refer to E as a *rectangle*.

We denote the left and right boundaries $\partial_l E$ and $\partial_r E$ of E by $\partial_l E = P(\{-1\} \times [-1, 1])$ and $\partial_r E = P(\{1\} \times [-1, 1])$, and call $\partial_v E := \partial_l E \cup \partial_r E$ the vertical boundary of E.

Likewise we introduce the horizontal boundary $\partial_h E := P([-1, 1] \times (\{-1\} \cup \{1\}))$ of E. These notions may be visualized in Fig. 1.

A *full-width* curve in E is a the image J of an embedding $\gamma : [-1, 1] \to E$ such that J is disjoint from $\partial_h E$ and meets each of $\partial_l E$ and $\partial_r E$ in single points.

We are interested in obtaining a rectangle E which forms a tight enclosure of the local unstable manifold W^u_E and for which W^u_E is a full-width curve.

The following theorem gives sufficient conditions for this.

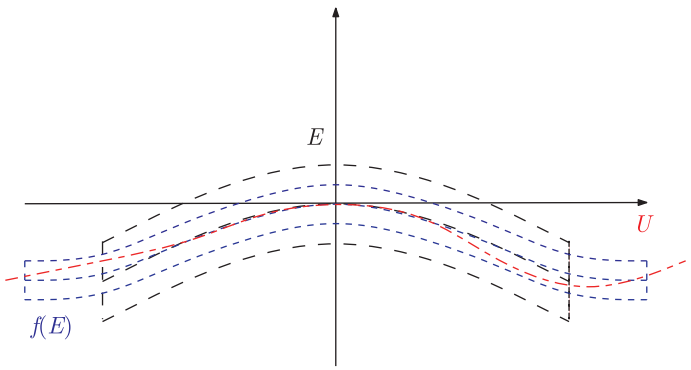

Fig. 1. A parameterized rectangle E (black, dashed), and its image (blue, dotted). In the situation of Theorem 2, the true local unstable manifold U (red, dash-dotted) is narrowly bounded in its transverse direction by both E and $f(E)$.

Theorem 2. *Let $\gamma(t) = (\gamma_1(t), \gamma_2(t))$, $t \in [-1, 1]$ be a regular curve with $\gamma_i(0) = 0$ for $i = 1, 2$. For $\epsilon > 0$, let $P(x, y) = (\gamma_1(x), \gamma_2(x) + \epsilon y)$, $x, y \in [-1, 1]$ and E be the image of P. Furthermore, let $f : E \to \mathbb{R}^2$ be a planar diffeomorphism as in Section 2.*

If

$$f(E) \cap \partial_h E = \emptyset, \tag{3.3}$$

then W^u_E is disjoint from $\partial_h E$.

If, in addition, there exists $M > 1$ and $S > 0$ such that, for all $z \in E$ and for all $s \in [-S, S]$ we have both

$$|\partial_1 f_2(z) + \partial_2 f_2(z) \cdot s| \leqslant S \text{ and } |\partial_1 f_1(z) + \partial_2 f_1(z) \cdot s| \geqslant M \tag{3.4}$$

then W_E^u is a full-width curve in E.

Proof. Let $\gamma(t)$, $t \in [-1, 1]$, be some parametrization of W_E^u with $\gamma(0) = (0, 0)$. Suppose W_E^u intersects $\partial_h E$. Let $K = \{t \in [-1, 1] \mid \gamma(t) \in \partial_h E\}$. Then, by continuity of W_E^u, there is a minimum $t_0 \in K$ such that $|t_0| \leqslant |t|$ for all $t \in K$.

Let $p = \gamma(t_0)$. Then the open arc $A \subset W_E^u$ connecting $(0, 0)$ and p lies in the interior of E. Since the unstable eigenvalue λ_u is positive, it follows that $f^{-1}(p)$ lies in the interior of A which, of course, is in E. This implies that p is in $f(E)$ which contradicts assumption (3.3).

To prove the second claim, let $\eta^0(t) = (\eta_1^0(t), \eta_2^0(t)), t \in [0, 1]$ be a parametrization of a piece of the unstable manifold satisfying the following conditions for all $t \in [0, 1]$:

$$\begin{aligned} \eta^0(0) &= (0, 0) \\ \left|s_{\eta^0}(t)\right| &< S \\ \dot{\eta}_1^0(t) &> 0. \end{aligned} \tag{3.5}$$

Note that such an η^0 certainly exists due to continuity in some small neighborhood around the fixed point, where the unstable manifold is tangent to the x-axis.

Let $\eta^1(t) = (\eta_1^1(t), \eta_2^1(t)) = f(\eta^0(t))$. We claim that if $\eta^0(t) \in E \; \forall t \in [0, 1]$, then η^1 again satisfies properties (3.5) and, furthermore, $\eta_1^1(t) \geqslant M\eta_1^0(t)$ for all $t \in [0, 1]$.

Clearly, η^1 is again a piece of the unstable manifold, and $\eta^1(0) = (0, 0)$. By the slope transformation law (3.2) and the conditions (3.4), we have that $\left|s_{\eta^1}(t)\right| < S \; \forall t \in [0, 1]$. Finally, by inserting $\eta^0(0) = (0, 0)$ and $s_{\eta^0}(0) = 0$ into the derivative transformation law (3.1), we have $\dot{\eta}_1^1(0) = \partial_1 f_1(0) \cdot \dot{\eta}_1^0(0) = \lambda_u \cdot \dot{\eta}_1^0(0) > 0$ since both λ_u and $\dot{\eta}_1^0(0)$ are positive. As η^1 has bounded slope, $\dot{\eta}_1^1$ is continuous and never zero, and thus has to be positive for all $t \in [0, 1]$.

As for the last claim, by the derivative transformation law (3.1) and the second condition (3.4), we have that $\left|\dot{\eta}_1^1(t)\right| > M \left|\dot{\eta}_1^0(t)\right|$. But since both $\dot{\eta}_1^1(t)$ and $\dot{\eta}_1^0(t)$ are positive for all $t \in [0, 1]$, we can drop the absolute values to find $\dot{\eta}_1^1(t) > M\dot{\eta}_1^0(t) \; \forall t \in [0, 1]$. Applying the fundamental theorem of calculus then yields

$$\eta_1^1(t) = \int_0^t \dot{\eta}_1^1(\tau) \, d\tau \geqslant \int_0^t M\dot{\eta}_1^0(\tau) \, d\tau = M\eta_1^0(t).$$

It follows that there exists some $k_0 \in \mathbb{N}$ such that $f^{k_0}(\eta^0)$ is not entirely in E any more. For assume no such k_0 existed. Then, by repeated application of the above, $f^k(\eta_1^0(1)) \geqslant M^k \eta_1^0(1) \; \forall k \in \mathbb{N}$. But since $M > 1$, and by assumption $f^k(\eta_1^0(1)) \in E \; \forall k \in \mathbb{N}$, this contradicts the compactness of E, as $M^k \eta_1^0(1)$ tends towards infinity for $k \to \infty$.

Let $\bar{k} \in \mathbb{N}$ be the smallest such k_0. By the above then $\eta^{\bar{k}} = f^{\bar{k}}(\eta^0)$ satisfies $\dot{\eta}_1^{\bar{k}}(t) > 0 \; \forall t \in [0, 1]$ and $\eta^{\bar{k}}(1) \notin E$. Consequently, the unstable manifold has to leave E through $\partial_r E$ since it cannot leave E through the horizontal boundaries. A similar argument holds for $\partial_l E$, i.e. the unstable manifold also leaves E through $\partial_l E$.

Let now $\gamma_0 : [-1, 1] \longrightarrow \mathbb{R}^2$ be a polynomial curve approximating W_E^u near the origin, $\gamma_0(0) = (0, 0)$, and assume that γ_0 is regular, a natural condition which can easily be checked rigorously. We will now use γ_0 to construct a suitable polynomial for the preceding theorem, and employ Taylor Model arithmetic to rigorously check the assumptions in guaranteeing the valid unstable curve enclosure.

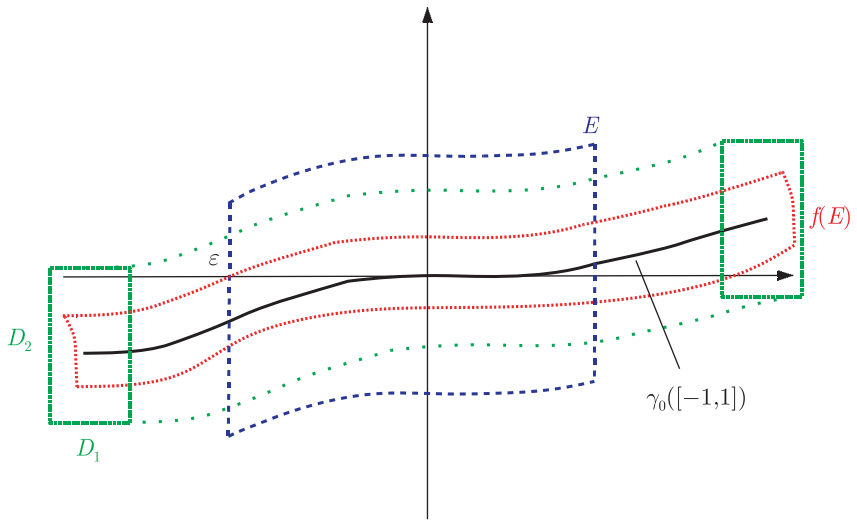

Fig. 2. The parameterized rectangle E (blue, dashed) is constructed around its center curve γ_0. The difference between γ_0 (black) and the iterate $f(E)$ (red, dotted) can be bounded by the interval box $D = (D_1, D_2)$ (green) such that $f(E) \subset \gamma_0([-1,1]) + D$.

Lemma 1. *For $\varepsilon > 0$, define the polynomial $P : [-1,1]^2 \longrightarrow \mathbb{R}^2$ as*

$$P(t,s) := \begin{pmatrix} \gamma_{0,1}(t) \\ \gamma_{0,2}(t) + \varepsilon \cdot s \end{pmatrix}, \tag{3.6}$$

and let $I_s, D_1, D_2 \subset \mathbb{R}$ be closed intervals such that

$$s_{\gamma_0}([-1,1]) \subset I_s, \tag{3.7}$$

as well as (cf. Fig. 2)

$$f(P(t,s)) \in \gamma_0(\lambda_u t) + D_1 \times D_2 \; \forall (t,s) \in \frac{[-1,1]}{\lambda_u} \times [-1,1] \tag{3.8}$$

Consider then the parameterized rectangle $E := P\left(\frac{[-1,1]}{\lambda_u}, [-1,1]\right)$. If

$$I_s \cdot D_1 - D_2 \subset (-\varepsilon, \varepsilon) \tag{3.9}$$

holds, then $f(E) \cap \partial_h E = \emptyset$ and condition (3.3) is satisfied if $\gamma(t) = \gamma_0(\frac{t}{\lambda_u})$ is used in Theorem 2.

Remark 3. The intuition behind the lemma is the following: if a polynomial curve γ_0 approximates the true local unstable manifold W_E^u well, then by thickening it slightly by a width ε, which in practice will be very small (10^{-12} and smaller), we obtain a thin parameterized rectangle P which has a chance to rigorously contain U. P mirrors the functional equation $f(W_E^u(t)) = W_E^u(\lambda_u t)$ of the true local manifold $W_E^u = W_E^u(t)$, i.e.

$$f(P(t,s)) \approx \gamma_0(\lambda_u t),$$

up to some small contributions of size less than ε, and the difference bounds D_i in (3.8) can be very sharp.

Proof. First note that E is indeed an embedded rectangle, since P is bijective and smooth and since E contains the fixed point, it also contains W_E^u. Now let p_0 be any point in E. Then $p_0 = P(t_0, s_0)$ for some $(t_0, s_0) \in \frac{[-1,1]}{\lambda_u} \times [-1,1]$. We want to show that $f(p_0)$ cannot be in the top boundary of E.

By condition 3.8 we have that

$$f_1(p_0) = f_1(P(t_0, s_0)) \in \gamma_{0,1}(\lambda_u t_0) + D_1.$$

Consider now the restricted top boundary of E with x-coordinates in the interval $\gamma_{0,1}(\lambda_u t_0) + D_1$. Due to the bounded slope of γ_0, this restricted top boundary is a single connected curve segment, or the empty set.

Integrating the slope along this curve segment one finds, again by virtue of the bounded slope of γ_0, that the y-coordinates of the restricted top boundary lie within the interval $\gamma_{0,2}(\lambda_u t_0) + \epsilon + I_s \cdot D_1$.

Thus, the difference between the y-coordinates of the restricted top boundary and $f_2(p_0)$ is in the interval

$$\gamma_{0,2}(\lambda_u t_0) + \epsilon + I_s \cdot D_1 - (\gamma_{0,2}(\lambda_u t_0) + D_2) = \epsilon + I_s \cdot D_1 - D_2.$$

Thus, if $I_s \cdot D_1 - D_2 \subset (-\epsilon, \infty)$, then $f(p_0)$ cannot be in the top boundary of E.

An analogous argument holds for the bottom boundary of E, assuming the condition $I_s \cdot D_1 - D_2 \subset (-\infty, \epsilon)$, thus completing the proof.

With the last result we are now ready to verify the conditions in Theorem 2 using Taylor Model methods:

Corollary 1. *Let ε, γ_0, P and E as in Lemma 1, and consider the Taylor Models*

$$T(t,s) := P(t,s) + \begin{pmatrix}[0,0]\\ [0,0]\end{pmatrix} = \begin{pmatrix}\gamma_{0,1}(t)\\ \gamma_{0,2}(t) + \varepsilon \cdot s\end{pmatrix} + \begin{pmatrix}[0,0]\\ [0,0]\end{pmatrix}.$$

Let $\dot{\Gamma}_i(t) := \widetilde{\gamma}_i(t) + I_i$ be a Taylor Model enclosure of the derivative $\dot{\gamma}_{0,i}(t)$ for $i = 1, 2$, such that $0 \notin \dot{\Gamma}_1([-1,1])$.

Furthermore, let $I_s^*, D_1^*, D_2^* \subset \mathbb{R}$ be intervals such that

$$\frac{\dot{\Gamma}_2([-1,1])}{\dot{\Gamma}_1([-1,1])} \subset I_s^*,$$

$$f_i\left(T\left(\frac{[-1,1]}{\lambda_u}, [-1,1]\right)\right) - \gamma_0([-1,1]) \subset D_i^* \text{ for } i = 1, 2.$$

If

$$I_s^* \cdot D_1^* - D_2^* \subset (-\epsilon, \epsilon)$$

then $f(E) \cap \partial_h E = \emptyset$.

Proof. First note that $T(t,s)$ is an exact Taylor Model representation of the parameterized rectangle generating E as in Lemma 1. Further, the $\dot{\Gamma}_i(t)$ can be obtained by Taylor Model derivation, as the test curve γ_0 is constructed as a finite order polynomial. The rest follows directly from applying Lemma 1 using Taylor Model arithmetic.

Proposition 2. *In the setting of Theorem 2, let*

$$T(t,s) := P(t,s) + \begin{pmatrix}[0,0]\\ [0,0]\end{pmatrix} = \begin{pmatrix}\gamma_{0,1}(t)\\ \gamma_{0,2}(t) + \varepsilon \cdot s\end{pmatrix} + \begin{pmatrix}[0,0]\\ [0,0]\end{pmatrix},$$

be a Taylor Model representation generating the rectangle E as in Lemma 1. Assume that there are $S > 0$ and $M > 1$ such that there are interval range bounds on the derivatives over T given by

$$\max\left(\left|\partial_1 f_2\left(T\left(\frac{x}{\lambda_u}, y\right)\right) - \partial_2 f_2\left(T\left(\frac{x}{\lambda_u}, y\right)\right) \cdot [-S, S]\right|\right) < S,$$

$$\min\left(\left|\partial_1 f_1\left(T\left(\frac{x}{\lambda_u}, y\right)\right) - \partial_2 f_1\left(T\left(\frac{x}{\lambda_u}, y\right)\right) \cdot [-S, S]\right|\right) > M,$$

for all $(x,y) \in [-1,1] \times [-1,1]$ and where $|I|$ for an interval I denotes the interval containing the absolute values of each element of I. Then conditions (3.4) *hold.*

Proof. Straightforward application of Taylor Model arithmetic on (3.4).

Remark 4. Finding a suitable slope bound S is not hard in practice. Due to the hyperbolic structure in the vicinity of the fixed point the derivative $\partial_1 f_1$ typically is large, and $\partial_2 f_2$ typically is small in absolute value, so that the relations (3.4) may hold true even for large test values S. A good algorithm for finding S is to start with $S = \max I_s^*$ (cf. Corollary 1) and inflating that value by some factor greater than one until the conditions are satisfied.

Summing up this section, given an approximate test polynomial γ_0 and a thickening $\varepsilon > 0$ such that the Taylor Model interval range bounds in Corollary 1 and Proposition 2 are satisfied, then the true unstable curve leaves the thin parameterized rectangle E constructed as in Lemma 1 through its vertical, and not its horizontal boundary.

3.2. Example: the Hénon map

As an example for the constructions we have developed so far we consider the Hénon map

$$H_{a,b}(x_1, x_2) := \left(1 + x_2 - a x_1^2, b x_1\right). \tag{3.10}$$

Depending on the parameter choices for a and b, the map exhibits a wide range of dynamics (e.g., since $\det(DH) = -b$ everywhere, the parameter b determines volume contraction or expansion). The standard parameter values proposed by Hénon originally are $a = 1.4$ and $b = 0.3$. In this situation, H exhibits seemingly complicated dynamics and a strange attractor. There are two hyperbolic saddle points p_1 and p_2, and we consider the invariant manifold structure near $p_1 \approx (0.63, 0.18)$.

Subsequently we consider the conjugated Hénon map

$$\tilde{H}_{a,b}(t_1, t_2) = L^{-1} \circ H_{a,b} \circ L(t_1, t_2) \tag{3.11}$$

where L is an affine transformation taking $(0, 0)$ to p_1 and diagonalizing the Jacobian of $\tilde{H}_{a,b}$ at the origin.

L can be found analytically by considering the eigenvalues of $DH_{a,b}$ at p_1,

$$\lambda_{1,2} = -a\, p_{1,1} \mp \sqrt{(a\, p_{1,1})^2 + b} \Longrightarrow \lambda_1 \approx -1.92\,,\ \lambda_2 \approx 0.156$$

and their corresponding eigenvectors

$$\mathbf{e}_i = \left(\frac{\lambda_i}{b}, 1\right)^T,\ i = 1, 2.$$

With these, we can set up the transformation matrix $M_{a,b} = \left(\mathbf{e}_1\ \mathbf{e}_2\right)$ and the complete transformation $L(t_1, t_2) = p_1 + M_{a,b} \cdot (t_1, t_2)^T$.

Carrying out the computation of L, and evaluating equation (3.11) with our parameters yields the approximate linearly diagonalized Hénon map in the new coordinates as

$$\tilde{H}_{a,b}(t_1, t_2) \approx \begin{pmatrix} -1.92 & 0 \\ 0 & 0.156 \end{pmatrix} \cdot \begin{pmatrix} t_1 \\ t_2 \end{pmatrix} - \begin{pmatrix} 1.30 t_1^2 \ + \ 2.60 t_1 t_2 \ + \ 1.30 t_2^2 \\ 0.105 t_1^2 \ + \ 0.21 t_1 t_2 \ + \ 0.105 t_2^2 \end{pmatrix}.$$

In the code, all computations are carried out using verified computations, yielding a rigorous enclosure of the transformed map. Similarly, we can derive rigorous enclosures for the Jacobian of $\tilde{H}_{a,b}$ to be used in the cone argument.

Computing the local unstable and stable manifold TM-enclosures of order 20 as outlined in Section 4, and affinely transforming back into the natural coordinate system, yields TM-enclosures as depicted in Figure 3. The width of these enclosures is on the order of 10^{-12} for both the unstable and stable manifolds.

To demonstrate the effect of the computation order of the polynomials used, Tables 1 and 2 show the size of ϵ used in the construction to successfully produce a verified enclosure of fixed arc length. The width of the resulting enclosure in each case is of the same order of magnitude as ϵ. For orders 1 and 2 of the stable manifold the desired length could not be obtained with any epsilon.

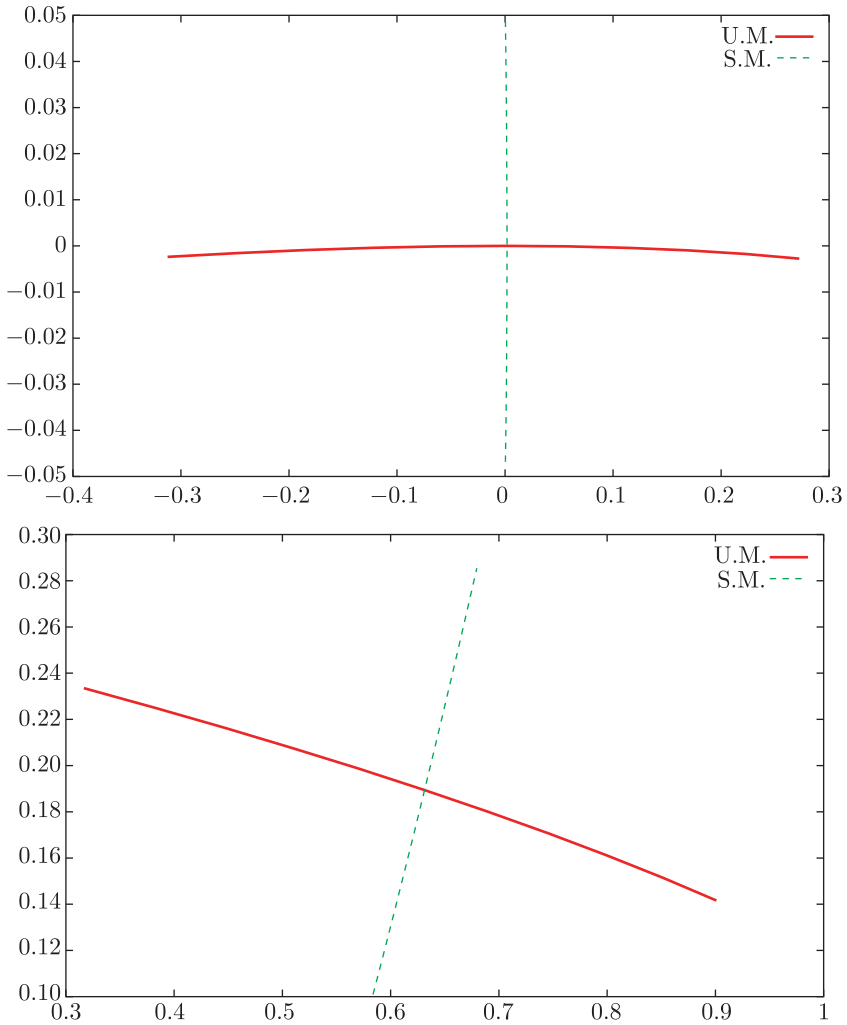

Fig. 3. Top: the enclosures of the local unstable (thin red) and stable (think green) manifold near the origin. Bottom: The same local manifold enclosures, but shifted around the fixed point $p_0 \approx (0.63, 0.18)$ and re-transformed into the original coordinate system.

This is caused by failure to verify the conditions of Proposition 2 in those cases. The only way to mitigate this is to reduce the length of the enclosure.

Conversely, in Tables 3 and 4 we fix ϵ and reduce the length of the enclosure until the verification succeeds.

Both tables show that the quality of the attainable enclosures increases vastly for orders up to about 10. Between orders 15 and 20, on the other hand, there is no improvement at all. This effect is caused by the errors due to limited floating point accuracy. For lower orders, the main source of errors is the poor approximation of the manifold by the polynomials. At higher orders, however, these approximation errors become so small, that the limited floating point accuracy becomes the main source for errors.

To obtain even better enclosures, high precision computations become necessary to reduce the size of the floating point errors.

4. GLOBAL MANIFOLD TANGLES

In the previous section we have demonstrated how the local invariant manifolds near a hyperbolic fixed point can be enclosed sharply using Taylor Model approximations. We can now proceed to generate significant pieces of the global manifold structure simply by iteration. Iterating the Taylor Model enclosures of the unstable manifold through the map f or the stable manifold enclosures

Table 1. Unstable manifold enclosures of fixed length (in natural coordinates) and the associated achievable width ϵ at different computation orders.

Order	Length	ϵ
1	0.59	$1.38 \cdot 10^{-2}$
2	0.59	$3.31 \cdot 10^{-3}$
3	0.59	$7.93 \cdot 10^{-4}$
4	0.59	$7.32 \cdot 10^{-5}$
5	0.59	$6.14 \cdot 10^{-6}$
6	0.59	$5.67 \cdot 10^{-7}$
7	0.59	$4.32 \cdot 10^{-8}$
8	0.59	$2.25 \cdot 10^{-9}$
9	0.59	$1.17 \cdot 10^{-10}$
10	0.59	$6.73 \cdot 10^{-12}$
15	0.59	10^{-12}
20	0.59	10^{-12}

Table 2. Stable manifold enclosures of fixed length (in natural coordinates) and the associated achievable width ϵ at different computation orders.

Order	Length	ϵ
1	0.16	0.14
2	0.19	$6.4 \cdot 10^{-2}$
3	0.21	$2.5 \cdot 10^{-3}$
4	0.21	$5.5 \cdot 10^{-5}$
5	0.21	$3.5 \cdot 10^{-7}$
6	0.21	$3.3 \cdot 10^{-9}$
7	0.21	$1.2 \cdot 10^{-11}$
8	0.21	$1.3 \cdot 10^{-12}$
9	0.21	$1.2 \cdot 10^{-12}$
10	0.21	$1.2 \cdot 10^{-12}$
15	0.21	$1.2 \cdot 10^{-12}$
20	0.21	$1.2 \cdot 10^{-12}$

Table 3. Unstable manifold enclosures of fixed epsilon and the associated achievable length (in natural coordinates) at different computation orders.

Order	Length	ϵ
1	$0.55 \cdot 10^{-5}$	10^{-12}
2	$0.48 \cdot 10^{-3}$	10^{-12}
3	$0.44 \cdot 10^{-2}$	10^{-12}
4	$0.18 \cdot 10^{-1}$	10^{-12}
5	$0.48 \cdot 10^{-1}$	10^{-12}
6	$0.99 \cdot 10^{-1}$	10^{-12}
7	0.17	10^{-12}
8	0.26	10^{-12}
9	0.38	10^{-12}
10	0.48	10^{-12}
15	0.59	10^{-12}
20	0.59	10^{-12}

Table 4. Stable manifold enclosures of fixed epsilon and the approximate achievable length (in natural coordinates) at different computation orders.

Order	Length	ϵ
1	$0.56 \cdot 10^{-6}$	10^{-12}
2	$0.90 \cdot 10^{-4}$	10^{-12}
3	$0.15 \cdot 10^{-2}$	10^{-12}
4	$0.91 \cdot 10^{-2}$	10^{-12}
5	$0.33 \cdot 10^{-1}$	10^{-12}
6	$0.83 \cdot 10^{-1}$	10^{-12}
7	0.16	10^{-12}
8	0.20	10^{-12}
9	0.20	10^{-12}
10	0.20	10^{-12}
15	0.20	10^{-12}
20	0.20	10^{-12}

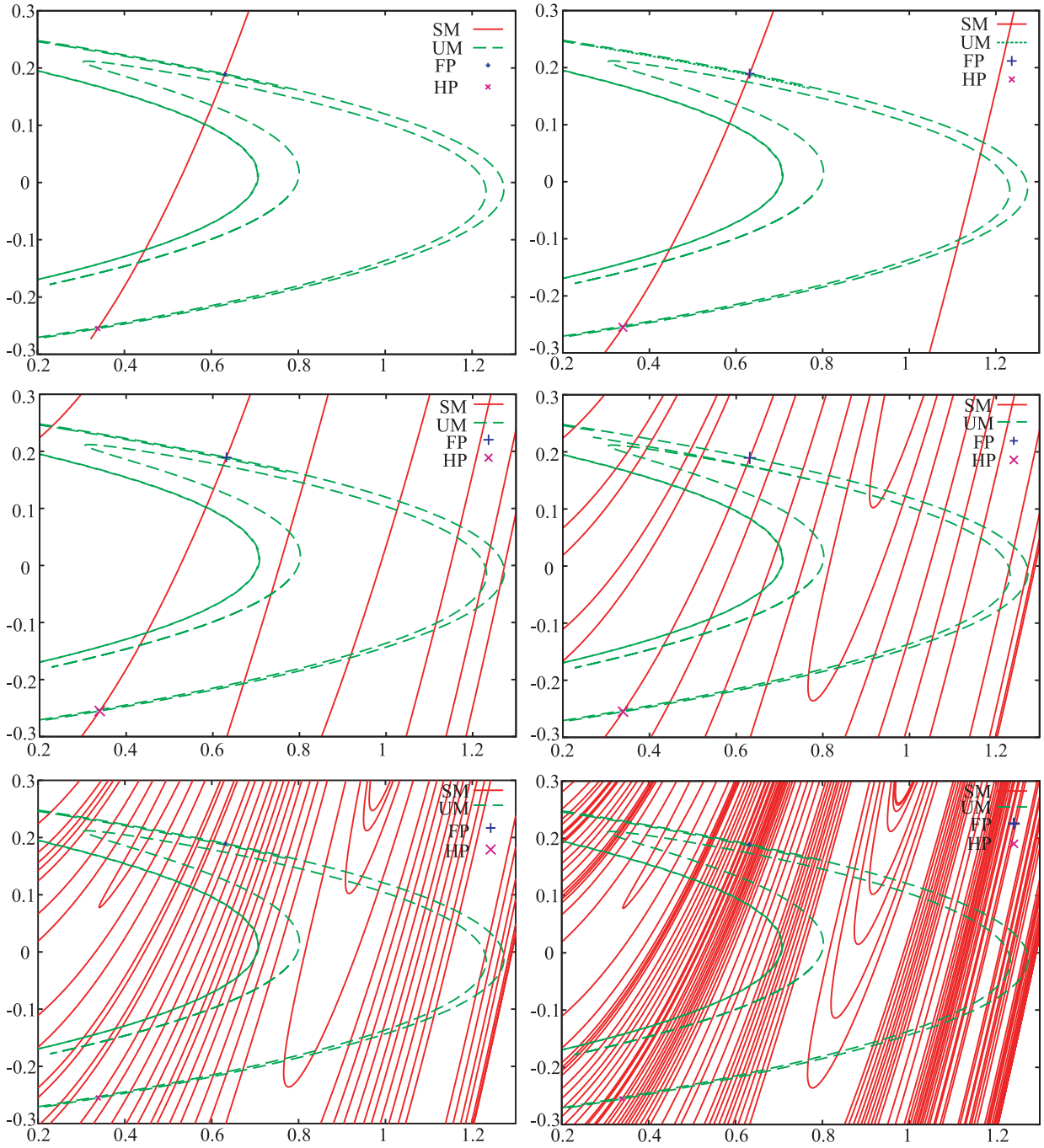

Fig. 4. 1st, 3rd, 5th, 7th, 9th, and 11th preimage of a local stable manifold enclosure (red) of the Hénon map $H_{a,b}$ for $a = 1.4$, $b = 0.3$, together with the unstable manifold (green). The actual Taylor Model enclosures are below printer resolution in width.

through the inverse f^{-1} in Taylor Model arithmetic will yield valid Taylor Model enclosures of successively larger global manifold pieces.

In practice, this approach requires a more involved and subtle treatment of the manifold pieces, even though the initial basic premise is retained in spirit. The fundamental problem is the quick blow-up of the remainder bound size under iteration. This is caused by two main factors.

Firstly, the remainder bound grows unproportionally if the truncation error between the true manifold and the polynomial part of the Taylor model enclosure becomes large. This is the case

when the manifold parametrization can only unsatisfactorily be modeled by a polynomial of fixed finite order, for instance when the true manifold grows exponentially in length under iteration, or if it makes sharp turns. Thus, the truncation error is primarily scaling with the longitudinally parameterizing variable of the Taylor model. The solution to keeping the truncation error size in check is to replace the single polynomial P by several polynomials obtained by bisection and rescaling as follows.

Algorithm 1. *Let $\tau = P_\tau(t,s) + I_\tau$ be a Taylor Model enclosure containing W^u_E, parameterized longitudinally by the variable t. Let $\delta > 0$ be the desired threshold of the C^0-approximation of $f(E^u_E)$ by the TM-enclosures, i.e. the maximal size of the remainder bounds. Let $M \in \mathbb{N}$ be the maximal number of bisection steps (typically $M < 10$). To generate TM-enclosures of new pieces of unstable manifold, execute the following algorithm:*

1. *Compute $f(\tau) =: P_{f(\tau)} + I_{f(\tau)}$ in Taylor Model arithmetic. If $\left|I_{f(\tau)}\right| \leqslant \delta$, the iteration is successful.*

2. *If $\left|I_{f(\tau)}\right| > \delta$, split and respirometric the TM τ as $\tau_1 := P_\tau\left(-\frac{1}{2} + \frac{t}{2}\right) + I_\tau$ and $\tau_2 := P_\tau\left(\frac{1}{2} + \frac{t}{2}\right) + I_\tau$, with $t \in [-1,1]$.*

3. *Compute $f(\tau_1) =: P_{f(\tau_1)}(t,s) + I_{f(\tau_1)}$ and $f(\tau_2) =: P_{f(\tau_2)}(t,s) + I_{f(\tau_2)}$. If $\left|I_{f(\tau_1)}\right| \leqslant \delta$ and $\left|I_{f(\tau 2)}\right| \leqslant \delta$, the iteration is successful.*

4. *If $\left|I_{f(\tau_1)}\right| > \delta$ or $\left|I_{f(\tau_2)}\right| > \delta$, repeat iteration from step 2.*

5. *If after M subdivisions not all remainder bounds are of width less than δ, either stop iteration or increase δ.*

The algorithm can be performed analogously for the stable manifold enclosures with the inverse map.

This algorithm generates an ordered list of local Taylor Model enclosures, the union of which still contains the true manifold, instead of one big Taylor Model which fails to sharply enclose the entire manifold iterate. While this particular algorithm only factors in the remainder bound size of the iterated manifold enclosures as the benchmark of where and how to bisect and reexpand the Taylor Model pieces, more sophisticated bisection methods can be implemented that take into account information like length, length growth or curvature.

Tables 5 and 6 illustrate the performance of this algorithm. For each iteration step performed, only pieces intersecting the box $[-1.5, 1.5] \times [-0.5, 0.5]$, which contains the attractor, are considered. The number of pieces, total length and the largest width are shown for the unstable and stable manifold respectively. All computations were done with Taylor Models of order 20.

While the number of pieces grows quickly to almost 4500 after 12 iterations of the stable manifold, this method still produces relatively sharp enclosures of a very long piece of the manifold. The cutting and re-expansion is crucial to obtain global manifold tangles. Increasing the computation order to try to cover the same manifold piece with one single Taylor Model is futile. The order required to achieve the same accuracy would be extremely high and since the coefficients get small rapidly, also very high precision would be needed.

However, even cutting and re-expansion cannot prevent the remainder bound from growing as can be seen in Tables 5 and 6. If the manifold enclosed by the Taylor Model is repelling, this causes the entire neighborhood contained in the Taylor model enclosure to expand, and consequently the Taylor Model along with it. There really is no way to control this expansion and loss of accuracy is unavoidable. The only remedy to still obtain sharp results for high iterates is to have higher accuracy in the local approximation to start out with.

Table 5. Largest width and number of pieces for the first 12 iterates of the unstable manifold. Computations are performed at order 20.

Iteration	Pieces	Length	Largest width
1	8	1.10	$6.30 \cdot 10^{-14}$
2	16	1.89	$1.44 \cdot 10^{-13}$
3	31	3.05	$2.65 \cdot 10^{-13}$
4	58	5.86	$7.29 \cdot 10^{-13}$
5	112	10.2	$1.76 \cdot 10^{-12}$
6	212	15.4	$3.67 \cdot 10^{-12}$
7	369	23.0	$7.45 \cdot 10^{-12}$
8	619	35.0	$1.45 \cdot 10^{-11}$
9	1004	55.0	$3.24 \cdot 10^{-12}$
10	1579	90.4	$6.32 \cdot 10^{-11}$
11	2583	143	$1.42 \cdot 10^{-10}$
12	4116	231	$2.90 \cdot 10^{-10}$

Table 6. Largest width and number of pieces for the first 12 iterates of the stable manifold. Computations are performed at order 20.

Iteration	Pieces	Length	Largest width
1	9	0.91	$7.63 \cdot 10^{-14}$
2	31	2.60	$5.26 \cdot 10^{-13}$
3	64	4.86	$5.00 \cdot 10^{-12}$
4	98	9.03	$3.26 \cdot 10^{-11}$
5	145	14.4	$3.74 \cdot 10^{-10}$
6	261	23.8	$4.11 \cdot 10^{-9}$
7	451	38.4	$4.69 \cdot 10^{-8}$
8	695	58.7	$4.95 \cdot 10^{-7}$
9	1120	93.4	$5.72 \cdot 10^{-6}$
10	1763	150	$6.40 \cdot 10^{-5}$
11	2805	243	$7.23 \cdot 10^{-4}$
12	4532	392	$8.10 \cdot 10^{-3}$

5. COMPUTATION OF HOMOCLINIC POINT ENCLOSURES

In the preceding sections we have presented a technique to get verified TM-enclosures of the invariant manifolds near a hyperbolic fixed point p, as well as a propagation scheme which yields an ordered list of TMs which rigorously enclose finite forward (inverse) images of the unstable (stable) manifold pieces at p, up to a finite number of iterates.

In the following we will describe a simple way of computing sharp interval bounds of the homoclinic intersection points of these parts of the invariant manifolds of p, with the added advantage that the computation can be automated in a straightforward fashion. In other words, we are confident that this technique is suitable to compute all intersection points of fairly long pieces of the invariant manifolds of p. Naturally, the approach can readily be extended to compute heteroclinic intersection points of two stable and unstable manifold pieces belonging to two different hyperbolic fixed points, but for brevity we will only consider homoclinic intersections of the manifold tangle of a single fixed point p.

The knowledge about homoclinic points is of course valuable in itself, since there are numerous aspects in the study of hyperbolic and chaotic dynamics directly related to their existence, abundance and mapping properties. But for the purpose of this presentation, the added benefit is that the quality of a numerical approximation of a homoclinic point can readily be checked through various quantitative techniques, which will give us good tests to assess the accuracy of the TM-manifold-enclosures that are used to compute the homoclinic points in the first place.

5.1. Verification of Existence of Homoclinic Points

Assume we are given TM-enclosures of two pieces of the planar unstable and stable manifold which are known to intersect. Let these TMs be parameterized as $T_1(t,s) = P_1(t,s) + I_1$ and $T_2(t,s) = P_2(t,s) + I_2$, with t and s as longitudinal parameters respectively, where $(t,s) \in [-1,1]^2$.

We note that as representations of two-dimensional sets, P_1 and P_2 overlap over a range of parameters, as depicted in Fig. 5. However, as the Taylor Models enclosing the manifold pieces are very thin (i.e. the transverse width is several orders of magnitudes smaller than the length), as a first step we may assume there is a pair of parameters (t_0, s_0) for which $P_1(t_0, s_0) \approx P_2(t_0, s_0)$. There are straightforward ways how (s_0, t_0) can be determined sharply, for example making use of a two-dimensional global optimization problem minimizing the distance between T_1 and T_2, or

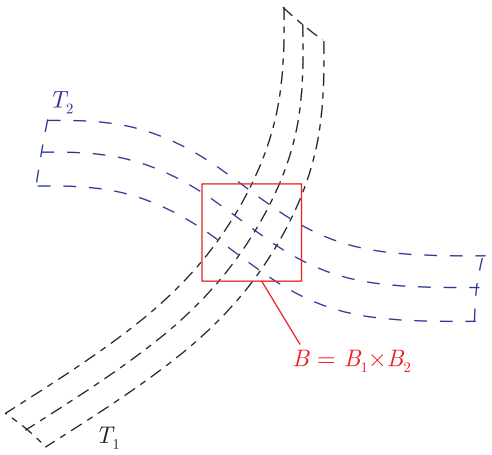

Fig. 5. Transverse crossing of two Taylor Models T_1 (dash-dotted) and T_2 (dashed). Their intersection can be enclosed into an interval box B (red, solid) which contains the homoclinic intersection of the true manifold pieces contained in T_1 and T_2.

a suitable Newton-type iteration once one is near the intersection point of the polynomial parts. Note that (t_0, s_0) need not be known rigorously.

Let us furthermore assume that T_1 and T_2 have been reexpanded around (t_0, s_0), so that their intersection point is close to the origin, and that we have performed a linear transformation on T_1 and T_2 with their inverse linear parts, which means that T_1 and T_2 are tangent to the x_1- and x_2-axes at the origin, respectively.

For easy of notation we also assume orientation such that

$$T_{1,1}(-1, s_0) < T_{1,1}(t_0, s_0) < T_{1,1}(1, s_0),$$
$$T_{2,2}(t_0, -1) < T_{2,2}(t_0, s_0) < T_{2,2}(t_0, 1),$$

but the following algorithm can easily be generalized to arbitrary orientations. We use $T_{i,j}$ for the jth component of the TM T_i, i.e. $T_{i,j} = P_{i,j}(t, s) + I_{i,j}$.

Algorithm 2. *First check that*

$$\left(\max\left(T_{1,1}\left(\{-1\} \times [-1,1]\right)\right) < \min\left(T_{2,1}\left([-1,1]^2\right)\right)\right)$$
$$\wedge \left(\max\left(T_{2,1}\left([-1,1]^2\right)\right) < \min\left(T_{1,1}\left(\{1\} \times [-1,1]\right)\right)\right)$$

and that

$$\left(\max\left(T_{2,2}\left([-1,1] \times \{-1\}\right)\right) < \min\left(T_{1,2}\left([-1,1]^2\right)\right)\right)$$
$$\wedge \left(\max\left(T_{1,2}\left([-1,1]^2\right)\right) < \min\left(T_{2,2}\left([-1,1] \times \{1\}\right)\right)\right)$$

Then the intersection contains a homoclinic point h. Furthermore, we can sharpen the interval enclosure of h by iterating the following algorithm:

1. *Compute the range bound in x_1-direction $T_{2,1}\left([-1,1]^2\right)$.*
2. *If there are $-1 < \theta_l < \theta_u < 1$ such that*

$$\left(\max\left(T_{1,1}\left([-1,\theta_l] \times [-1,1]\right)\right) < \min\left(T_{2,1}\left([-1,1]^2\right)\right)\right)$$
$$\wedge \left(\max\left(T_{2,1}\left([-1,1]^2\right)\right) < \min\left(T_{1,1}\left([\theta_u,1] \times [-1,1]\right)\right)\right)$$

   reexpand T_1 around $t_1 \longrightarrow \frac{\theta_u - \theta_l}{2} + \frac{\theta_u - \theta_l}{4} t_1$.
3. *Repeat from step 1, but switch the indices 1 and 2 in both the TMs T_1, T_2 and their components, and the variables t and s.*
4. *Stop the algorithm if step 2 cannot be performed successfully or if the widths of $T_{1,1}\left([-1,1]^2\right)$ and $T_{2,2}\left([-1,1]^2\right)$ undercut the desired accuracy threshold.*

It is of note that the heuristic determination of $\theta_{l,u}$ in step 2 can be done very elegantly by using the map inversion tools which are available in the COSY implementation of DA-arithmetic [1]. The values

$$\theta_l \approx P_{1,1}^{-1}\left(\min(T_{2,1}([-1,1])^2),0\right),$$
$$\theta_u \approx P_{1,1}^{-1}\left(\max(T_{2,1}([-1,1])^2),0\right)$$

are a good initial guess for $\theta_{l,u}$, possibly after a slight inflation by 10 percent or so.

As a side note, the algorithm can be extended to determine the parametrization orientation of the manifolds at a given homoclinic point, which, while not relevant for the results published in this paper, can be used for more advanced studies of homoclinic tangles.

To give an example for the performance of the last algorithm we return to the Hénon map. We can enclose specific homoclinic points as follows:
In the global manifold tangle constructed in the previous section we see that successive iteration of the TM-enclosures of the local stable and unstable manifolds at the fixed point p_1 through the map $H_{a,b}$ or the inverse $H_{a,b}^{-1}$ seems to generate the "first" (in the sense of arclength) homoclinic intersection point of the iterated TM-enclosures, which we call q_1, at about $(0.33, -0.25)$. Applying the above sharpening algorithm, we are able to assert existence of such a point in a quite sharp interval box enclosure of width $\approx 10^{-12}$:

Theorem 3. *In the standard Hénon map (3.10), the transverse homoclinic intersection q_1 of W^u and W^s of the hyperbolic fixed point $p_1 \approx (0.63, 0.18)$ is contained within the interval box*

$$([0.338852549387, 0.33885254939], [-0.255112629783, -0.2551126297832]). \tag{5.1}$$

5.2. Numerical Tests

The rigorous homoclinic point enclosures from the last section serve as an excellent litmus test for the claimed accuracy of the manifold enclosure themselves, and various *a posteriori* tests to check the quality of the homoclinic point enclosure can be performed to support the sharpness of the interval enclosure. Unfortunately, no analytic formula for the coordinates of the true homoclinic point of the Hénon map near $(0.35, -0.25)$ exist, so we have to resort to some nonverified, but quantitative numerical experiments to corroborate the statement 3.

In the following we assume that p is a hyperbolic fixed point of a planar diffeomorphism $f : \mathbb{R}^2 \longrightarrow \mathbb{R}^2$ with eigenvalues $0 < |\lambda_2| < 1 < |\lambda_1|$ of $Df_p(0)$, h_t is a true homoclinic point in $W_p^s \cap W_p^u$, and h_c is a computed numerical approximation of h_t. It is clear that there are completely analogous method to estimate the displacement of h_c from the unstable manifold by correspondingly using f^{-1} instead of f.

Theorem 3 must hold true by virtue of every step in algorithm (2) having been performed in Taylor Model arithmetic. However, there are nonverified numerical techniques that can substantiate the claim of the theorem in an intuitive manner. Define the midpoint of the homoclinic point enclosure (5.1) as

$$h_c := (0.3388525493875, -0.25511262978315), \tag{5.2}$$

and let h_t be a the true homoclinic point q_1 contained in (5.1).

5.2.1. Number of Forward Iterates Near Fixed Point as a Measure

The first very simple and straightforward method to measure the quality of h_c is the number of forward iterates that stay within a neighborhood of p. Since h_c is close to h_t, the images $f^k(h_c)$ first converge to p_1 along the stable manifold and, once near p_1, get pulled away from p_1 again along W_p^u with a factor of $\approx |\lambda_1|$ in every iteration for the distance to W_p^s. If we consider the maximal number K of iterations such that the forward iterates $f^k(h_c)$ do not leave a ball $B_\delta(p)$ for $k \leqslant K$ (where δ is reasonably small, say $\delta \approx 0.1$), then we know that the original displacement of h_c from W_p^s, or from h_t respectively, can be approximately be expressed as

$$d(h_c, h_t) \approx \operatorname{dist}(h_c, W_p^s) \approx \frac{\delta}{|\lambda_1|^K}. \tag{5.3}$$

In the example above with $f = H_{a,b}$, $|\lambda_1| \approx 1.92$ and $\delta = 0.1$, we get $K = 40$, i.e.

$$d(h_c, h_t) \approx 0.1/(1.92)^{40} \approx .4655 \cdot 10^{-13} \tag{5.4}$$

which is compatible with the claimed sharpness of the enclosure from Theorem 3.

5.2.2. Monitoring of Distance to Stable Manifold Under Forward Iteration

The second method is very much similar in spirit to the first one, but with a more accurate numerical result for the original displacement of h_c from W_p^s, and hence h_t. The reason why the first method only gives a rough estimate about $d(h_c, h_t)$ is that the expansion of the distance of $f^k(h_c)$ to the stable manifold only goes with a factor of $|\lambda_1|$ in the higher iterates where $k \approx K$, i.e. where $f^k(h_c)$ is near p. For the lower iterates with small k, while there still is expansion of $dist(f^k(h_c), W_p^s)$ in principle due to the hyperbolic structure of the system near W_p^s, that expansion factor need not be $|\lambda_1|$, which when combined as in eq.(5.3) can produce errors in the range of one order of magnitude.

The approach for a more plausible estimate of $d(h_c, h_t)$ is to monitor the contraction of $dist(f^k(h_c), W_p^s)$ for every iterate $0 \leqslant k \leqslant K$, and keep track of all shrinking factors. In the following we outline the algorithm:

1. Let $\gamma(t)$ be the polynomial part of the TM-enclosure of W_p^s between h_t and p. Define $h_0 := h_c$.

2. For $0 \leqslant n \leqslant K-1$: Let $h_n := f(h_{n-1})$. Compute the perpendicular unit vector u_n from h_n to γ by minimizing the scalar product $|\langle \dot\gamma(t), \gamma(t) - h_n \rangle|$ over the parameter t at t_n. Set $u_n := (\gamma(t_n) - h_n) \cdot (|\gamma(t_n) - h_n|)^{-1}$. Evaluate the Jacobian $Df(h_n)$ and compute the length growth factor $k_n := |Df(h_n) \cdot u_n|$.

3. Approximate $d(h_c, h_t) \approx dist(h_K, W_p^s) \cdot \left(\prod_{n=0}^{K-1} k_n \right)^{-1}$.

In our present case with h_c as in (5.2), $h_t = q_1$ and $K = 40$ we obtain a numerical value

$$d(h_c, h_t) \approx 0.897 \cdot 10^{-13}$$

which is again in agreement with the previous rigorous claim.

5.2.3. Mapping to Different Sides of the Stable Manifold

Considering the computed point h_c and the tangent direction of the stable manifold near h_c, we can construct another point $\tilde h_c$ that has been translated perpendicularly to the manifold tangent from h_c by a small (positive or negative) length l roughly of the size of the expected displacement $dist(h_c, W_p^s)$. If indeed the points h_c and $\tilde h_c$ lie on different sides of the manifold, then so will all their forward iterates. In other words, once the points $f^k(h_c)$ and $f^k(\tilde h_c)$ get near p, their images slowly drift away from each other to follow different branches of the unstable manifold under subsequent iteration, which can be observed by simply printing the iterates of both points to the screen. If this diverging behavior of $f^k(h_c)$ and $f^k(\tilde h_c)$ persists, the true set W_p^s has to be within $|l|$ of h_c.

Returning to the claimed homoclinic point interval enclosure in Theorem 3, its top left and right cornerpoints were mapped successively by the squared Hénon map $H_{a,b}^2$ (to avoid confusing switching of sides of the iterates) as depicted in Fig. 6a. Likewise, Fig. 6b) shows the iterates by $H_{a,b}^{-2}$ of the right top and bottom cornerpoints of the interval box. In both cases we see that the iterates follow different branches of the unstable and stable manifold near the fixed point, respectively, which is again compatible with the claim of Theorem 3.

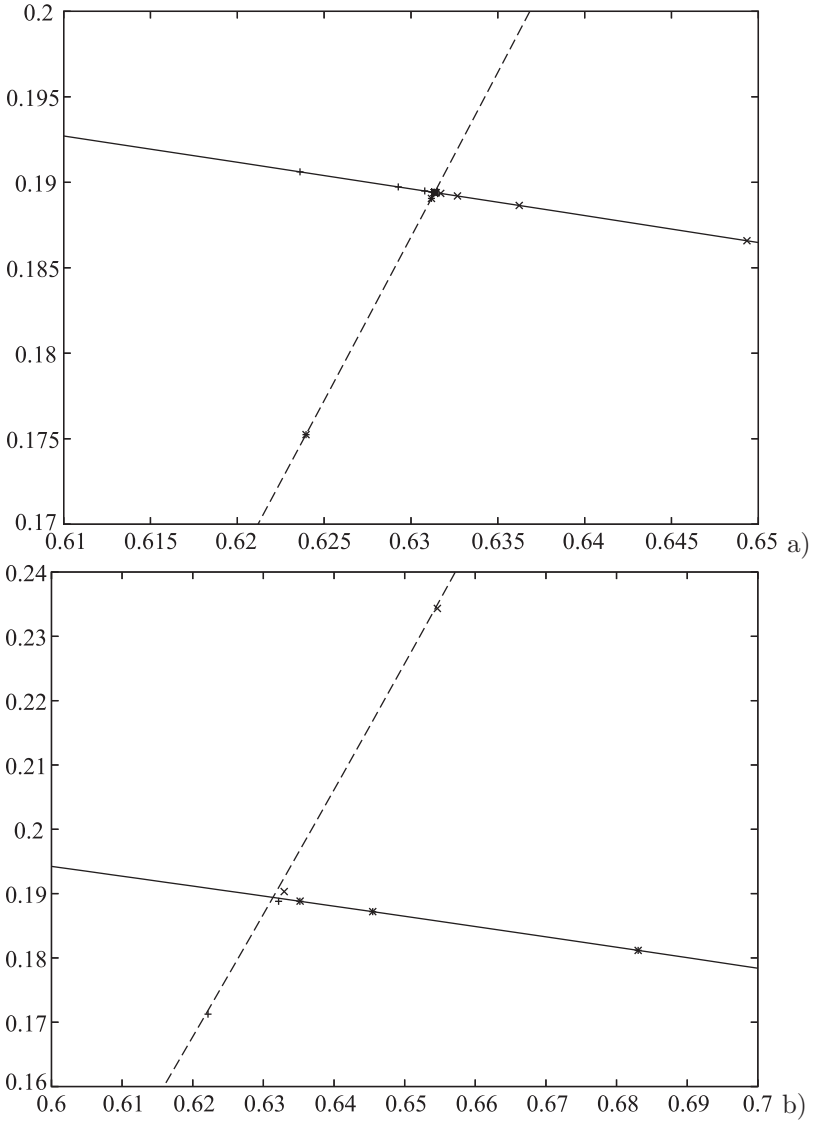

Fig. 6. (a) The first 20 iterates of H^2 of the left (plus) and right (x) top cornerpoints of the claimed homoclinic point interval enclosure from Theorem (3) are plotted. (b) The first 10 iterates of H^{-2} of the top (plus) and bottom (x) right cornerpoint of the same interval box enclosure are plotted. The unstable manifold is drawn solid, the stable manifold dashed.

REFERENCES

1. Berz, M., *Modern Map Methods in Particle Beam Physics*, San Diego: Academic Press, 1999; also available at http://bt.pa.msu.edu/pub.
2. Berz, M. and Makino, K., Verified Integration of ODEs and Flows Using Differential Algebraic Methods on High-Order Taylor Models, *Reliable Computing*, 1998, vol. 4, no. 4, pp. 361–369.
3. Berz, M. and Makino, K., Suppression of the Wrapping Effect by Taylor Model-based Verified Integrators: Long-term Stabilization by Shrink Wrapping, *Int. J. Differ. Equ. Appl.*, 2005, vol. 10, pp. 385–403.
4. Cabré, X., Fontich, E., and de la Llave, R., The Parametrization Method for Invariant Manifolds I: Manifolds Associated to Non-resonant Subspaces, *Indiana Univ. Math. J.*, 2003, vol. 52, pp. 283–328.
5. Cabré, X., Fontich, E., and de la Llave, R., The Parametrization Method for Invariant Manifolds II: Regularity with Respect to Parameters, *Indiana Univ. Math. J.*, 2003, vol. 52, pp. 329–360.
6. Fornaess, J. and Gavosto, E., Tangencies for Real and Complex Hénon Maps: An Analytic Method. *Experiment. Math.*, 1999, vol. 8, no. 3, pp. 253–260.
7. Franceschini, B. and Russo, C., Stable and Unstable Manifolds of the Hénon Mapping, *J. Stat. Phys.*, 1981, vol. 25, no. 4, pp. 757–769.

8. Hubbard, J., Parametrizing Unstable and Very Unstable Manifolds, *Mosc. Math. J.*, 2005, vol. 5, no. 1, pp. 105–124.
9. Makino, K., *Rigorous Analysis of Nonlinear Motion in Particle Accelerators*, PhD thesis, East Lansing, Michigan: Michigan State University, 1998.
10. Makino, K. and Berz, M., Remainder Differential Algebras and Their Applications, in M. Berz, C. Bischof, G. Corliss, and A. Griewank (Eds.), *Computational Differentiation: Techniques, Applications, and Tools (Santa Fe, NM, 1996)*, Philadelphia: SIAM, 1996, pp. 63–74.
11. Makino, K. and Berz, M., Taylor Models and Other Validated Functional Inclusion Methods, *Int. J. Pure Appl. Math.*, 2003, vol. 6, no. 3, pp. 239–316.
12. Makino, K. and Berz, M., Suppression of the Wrapping Effect by Taylor model-based Verified Integrators: Long-term Stabilization by Preconditioning. *Int. J. Differ. Equ. Appl.*, 2005, vol. 10, no. 4, pp. 253–384.
13. Makino, K. and Berz, M., Suppression of the Wrapping Effect by Taylor Model-based Verified Integrators: The Single Step, *Int. J. Pure Appl. Math.*, 2006, vol. 36, no. 2, pp. 175–187.
14. Moore, R.E., *Methods and Applications of Interval Analysis*, Philadelphia: SIAM, 1979.
15. Revol, N., Makino, K., and Berz, M., Taylor Models and Floating-Point Arithmetic: Proof that Arithmetic Operations are Validated in COSY. *J. Log. Algebr. Program.*, 2005, vol. 64, no. 1, pp. 135–154.